# Hierarchical organization of brain functional networks during visual tasks

Zhao Zhuo,[1] Shi-Min Cai,[1,*] Zhong-Qian Fu,[1,†] and Jie Zhang[2,‡]

[1]*Department of Electronic Science and Technology, University of Science and Technology of China, Hefei Anhui 230026, People's Republic of China*

[2]*Centre for Computational Systems Biology, Fudan University, Shanghai 200433, People's Republic of China*

(Received 24 January 2011; revised manuscript received 14 August 2011; published 22 September 2011)

The functional network of the brain is known to demonstrate modular structure over different hierarchical scales. In this paper, we systematically investigated the hierarchical modular organizations of the brain functional networks that are derived from the extent of phase synchronization among high-resolution EEG time series during a visual task. In particular, we compare the modular structure of the functional network from EEG channels with that of the anatomical parcellation of the brain cortex. Our results show that the modular architectures of brain functional networks correspond well to those from the anatomical structures over different levels of hierarchy. Most importantly, we find that the consistency between the modular structures of the functional network and the anatomical network becomes more pronounced in terms of vision, sensory, vision-temporal, motor cortices during the visual task, which implies that the strong modularity in these areas forms the functional basis for the visual task. The structure-function relationship further reveals that the phase synchronization of EEG time series in the same anatomical group is much stronger than that of EEG time series from different anatomical groups during the task and that the hierarchical organization of functional brain network may be a consequence of functional segmentation of the brain cortex.

DOI: 10.1103/PhysRevE.84.031923 PACS number(s): 87.19.lj, 87.19.le, 87.19.lt, 89.75.Fb

## I. INTRODUCTION

The human brain, which consists of ten thousand million neurons and even more synapses, is perhaps the most complex system ever known. Benefiting from the development of brain anatomy since the 19th century, we now know that the neuronal elements of the brain constitute an extremely complex structural network, which subserves a wide variety of cognitive functions and neural activities [1–3]. Recently, it has gained great interests among scientists to investigate the functional connectivity of brain based on complex network theory in which the brain can naturally be abstracted as a functional network. A brain functional network can be extracted based on functional MRI (fMRI), electroencephalography (EEG), magnetoencephalography (MEG), or multielectrode array (MEA) data, which record electric, magnetic, or other signals representing cortical activities of the brain [4]. Vertices of brain functional network derived from fMRI data describe anatomically localized regions of interest (ROIs) or voxels of fMRI image, whereas the vertices of those derived from EEG, MEG, or MEA data denote surface electrodes or sensors. The functional connectivity (or edge) between pairs of vertices is usually estimated using correlation between time series recordings of the vertices.

It has been widely observed that the brain functional networks demonstrate properties such as small-worldness [5] and power-law degree distribution [6], which distinguish themselves from regular and random networks [7–12]. However, the small-worldness and power-law degree distribution represent only the global properties of brain functional networks. To understand brain functional networks imposed by structural and functional constraints more comprehensively, the hierarchical modular organization, which can reflect both local and global organization of brain functional network, should be fully investigated.

Hierarchical organization, also called community structure and modular architecture, describes the fact that some nodes in a network are densely connected as groups, and these groups are only sparsely connected among themselves, which is a common phenomenon in diverse networks such as World Wide Web, scientist collaboration networks, genetic networks, protein-protein interaction networks, and financial networks [13–16]. A large number of algorithms have been developed to detect the hierarchical organizations of real networks [13,17–23] (also see the review in Ref. [24]). Interestingly, several recent works have also found the hierarchical organization of the brain functional networks derived from resting-state fMRI data [25,26] and epileptic MEG signals [27], respectively.

Although there are many works devoted to the hierarchical organization of the brain functional networks, most of them are confined to the " resting state." The study of this organization in the "task state" and the investigation of its functional implications are rare. In this paper, we analyzed the brain functional networks of the subjects during the visual task which involves visual, sensory, and motor functions of the brain cortex. In our work, the brain functional networks are derived from high-resolution synchronous EEG time series, which consist of 238 channels and are recorded during the visual task. In the functional network, the vertices correspond to surface electrodes (i.e., channels), while edges are determined by the extent of phase synchronization of EEG time series from pairs of channels, and we first analyze the community structure of the brain functional networks by the fast Girvan-Newman (GN) algorithm (i.e., functional cluster). On the other hand, these electrodes can also be assigned into the same group by their spatial positions on scalp and *a priori*

*csm1981@mail.ustc.edu.cn
†zqfu@ustc.edu.cn
‡jzhang080@gmail.com

 

knowledge of anatomical parcellation of the brain cortex (i.e., anatomical clusters). For instance, electrodes near the visual cortex area mainly represent visual function and, therefore, these electrodes can also be clustered together in this manner. The anatomical parcellation of brain cortex is performed according to the Brodmann segmentation scheme [28].

Comparing the community structure of the brain functional network and that of the anatomical segmentation, we find that there is a significant coincidence between the modular architecture of the network derived from EEG data and that from the anatomical organization of the cortex over different levels of hierarchy. Furthermore, this coincidence turns out to be more pronounced at the vision, sensory, vision-temporal, and motor cortices of the brain during the visual task. This result shows that vertices are more tightly coupled in the same functional regions than those belonging to different ones, and this is more evident in the vision, sensory, vision-temporal, and motor cortices during the visual task. Our results suggest that the patterns of neural activities of brain cortex in the task are, to a large extent, determined by the anatomical, modular architecture of the brain, and this anatomical structure forms the functional basis of the brain during the task.

## II. MATERIALS AND METHODS

### A. Data acquisition

The high-resolution EEG time series were synchronously recorded during the visual task by using a large number of scalp electrodes (238 channels), which had a high spatial and temporal resolution that can provide detailed information of electrical activities of the cortical surface. This data set was recorded by A. Delorme *et al.* at the Swartz Center at the University of California at San Diego, with a sampling rate of 256 Hz (using a Biosemi Active Two system [29]). To further minimize the artificial responses from line noise, it was digitally low pass filtered below 40 Hz before data analysis. The experiments were performed as follows: In each session, 120 stimuli (filled white disks) were briefly displayed for 100 ms inside one of the five empty squares in a pseudorandom order with interstimuli intervals being 250–900 ms, and one of the five outlines was colored green to mark the square as a visual target, and then the candidate made a motor response by pressing a mouse button with their right hand as quickly as possible whenever the filled white disk appeared at the attended location. It is noted that each visual target was recorded by a synchronous EEG time series with five sessions of trials, and the candidate was given breaks between sessions. The more detailed description of the experiment can be found in several previous works [30,31]. In this data set, a total of 25 sessions were therefore collected, and about 3000 trials of experiment were performed. In addition, there are 235 channels of EEG used in our work by dropping 3 channels of EOG.

### B. Network construction based on phase synchronization

The concept of phase synchronization is introduced to study synchronization of coupled oscillators and has gained particular interests to investigate coupling among nonlinear complex systems [32–34]. The phase $\Phi(t)$ of a real-value time series $X(t)$ is defined using Gabor's analytic signal approach [35]:

$$V(t) = X(t) + iX_h(t) = Ae^{i\Phi(t)}, \tag{1}$$

where the imaginary part $X_h(t)$ is the Hilbert transformation of $X(t)$. Hence, the degree of phase synchronization between time series $X_i(t)$ and $X_j(t)$ can be evaluated by a bivariate phase-coupling index [36,37]:

$$R_{i,j} = \left\| \frac{1}{T} \sum_{t=1}^{T} e^{i(\phi_i(t)-\phi_j(t))} \right\|, \tag{2}$$

which is in the interval [0, 1]. If the phases of two time series are completely synchronized, then the phase-coupling index will be at maximum.

One advantage of phase synchronization is that it can reduce the nonstationary effect in EEG time series compared with linear correlation. The functional connectivity (edge) between pairs of electrodes (vertices) is first estimated using the measure of phase synchronization, and then it is thresholded to generate a binary functional network. Herein each vertex is connected to its $N$ nearest neighbors (i.e., those channels that are most phase synchronized with it) [38]. Note that the resulting brain functional networks are not necessarily symmetric, i.e., if vertex $i$ is a neighbor of vertex $j$, vertex $j$ may not necessarily be a neighbor of vertex $i$ and vice versa. Here we take the network as an undirected network for convenience. The mean degree of network is generally determined by $N$. However, since the directed edges are identified as undirected ones, the actual mean degree is a little larger than $N$. In this way, the connectivity of brain functional network is naturally guaranteed without dense connections, which will otherwise disturb the hierarchy detection.

### C. Clustering EEG channels by both the GN algorithm and the anatomical parcellation of the brain

The EEG time series recorded through each channel mainly represents the electrical activities of neurons near the corresponding electrode. Thus, the EEG channels can be directly clustered into groups according to the spatial position of electrodes and anatomical parcellation of brain cortex (e.g., Brodmann segmentation scheme). We used the Brodmann template image distributed with MRIcro, which is restricted to the standard MNI space [39]. Resolution of the image is $181 \times 217 \times 181$ and the size of voxels is $1 \times \times 1 \times 1$ mm. Each hemisphere is partitioned into 41 areas according to Brodmann segmentation scheme, with the same label suggesting the same functional area of brain cortex in two hemispheres. The 3D-coordinate locations of electrodes are mapped to the standard MNI space using SPM8 toolbox (open-source software) [40]. Hence, we can achieve the mapping relation between electrodes and Brodmann areas by matching the 3D coordinates in the standard MNI space. The EEG electrodes that lie in the same Brodmann area are clustered together (i.e., labeled by the same Brodmann area index). At last, these 235 channels are clustered into 25 anatomical groups corresponding to 25 Brodmann areas. Some Brodmann areas are absent in this case because they are

TABLE I. Number of EEG channels restricted to each Brodmann area.

| Brodmann area | EEG channel number | Brodmann area | EEG channel number |
|---|---|---|---|
| 20 | 29 | 4 | 7 |
| 19 | 26 | 10 | 7 |
| 6 | 19 | 8 | 5 |
| 18 | 16 | 22 | 5 |
| 9 | 14 | 38 | 5 |
| 37 | 13 | 44 | 5 |
| 45 | 12 | 43 | 4 |
| 40 | 11 | 48 | 4 |
| 7 | 10 | 1 | 3 |
| 21 | 9 | 2 | 3 |
| 46 | 9 | 5 | 2 |
| 17 | 8 | 47 | 1 |
| 39 | 8 | | |

deeply beneath the cortex where there are no corresponding EEG electrodes. The size of anatomical group (i.e., the number of electrodes it contains) varies from 1 to 29, as shown in Table I. Moreover, Brodmann areas can also be roughly scaled into 9 major substructures according to specific physiological functions, by which the EEG channels can be further clustered at this higher hierarchy, as shown in Table II. Hence, the EEG channels are organized into two levels of hierarchy according to the above-mentioned segmentation.

The hierarchical or modular organization of network from EEG channels can be analyzed in two ways: (i) the modular structure of brain functional networks that can be detected by fast GN algorithm and (ii) the modular structure of the EEG channels according to anatomical parcellation of brain cortex based on the Brodmann segmentation scheme. The former is a functional clustering structure and the latter is an anatomical clustering structure. Thus, the relationship between these two kinds of hierarchical/clustering structures (e.g., the overlap between the communities from both clustering structures) is a key question that is expected to shed light onto the relationship between the structure and function of the brain.

TABLE II. Number of EEG channels restricted to the anatomical substructure.

| Functional substructure | Brodmann area | EEG channel number |
|---|---|---|
| Broca's (B) | 44, 45 | 17 |
| Audition (A) | 22 | 5 |
| Cognition (C) | 9, 10, 46, 47 | 31 |
| Emotion (E) | 38 | 5 |
| Vision (V) | 17, 18, 19 | 50 |
| Vision-parietal (Vp) | 7, 39 | 18 |
| Vision-temporal (Vt) | 20, 21, 37 | 51 |
| Motor (M) | 4, 6, 8 | 31 |
| Sensory (S) | 1, 2, 5, 40 | 19 |

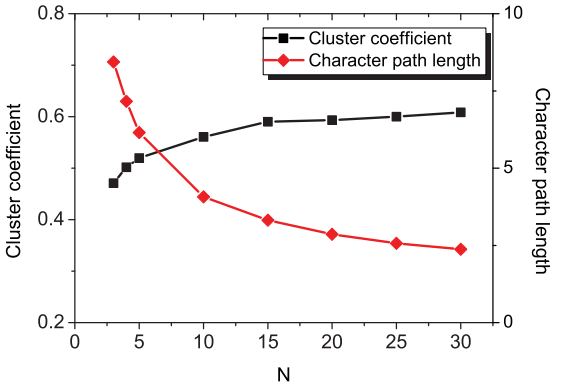


FIG. 1. (Color online) Average cluster coefficient and characteristic path length as a function of $N$.

## III. EMPIRICAL RESULTS

We calculate the phase-synchronization index matrix of all the sessions that consist of continuously recorded multichannel EEG time series. An average is performed over all 25 sessions. The brain functional networks then are generated using a tunable $N$ (the number of nearest neighbors). The average cluster coefficient (CC) and characteristic path length (CPL) are also computed as a function of $N$ (see Fig. 1), and we find that the brain functional networks behave large CC and short CPL, which suggests the small-world property in consistency with previous works.

Community structure and modular architecture are two crucial properties of brain functional networks during the visual task. The fast GN algorithm is applied to explore these hierarchical organizations of the brain functional networks. Results are shown in Fig. 2 for different $N$, of which the minimum value is 3. Figure 2 shows that the maximum modularity monotonously decreases with $N$, all above 0.5 even when $N \leqslant 30$, which obviously differs from that of the randomly connected network. Furthermore, small maximum modularity also corresponds to a large mean degree of network, which suggests that more edges bridge the communities to reduce gaps of clusters and render the community structure less visible. Obviously, the number of communities corresponding to maximum modularity is also a monotonously decreasing function of $N$. With these considerations in mind, we mainly

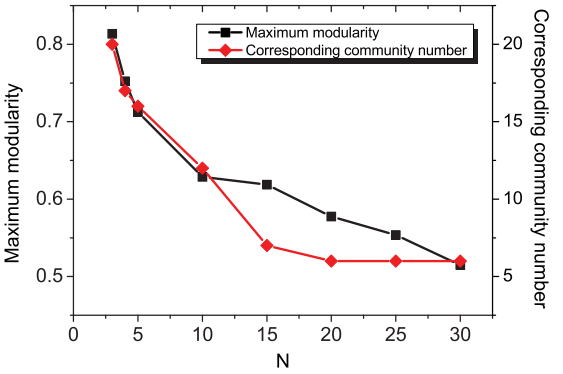


FIG. 2. (Color online) Maximum modularity and corresponding community number as a function of $N$.

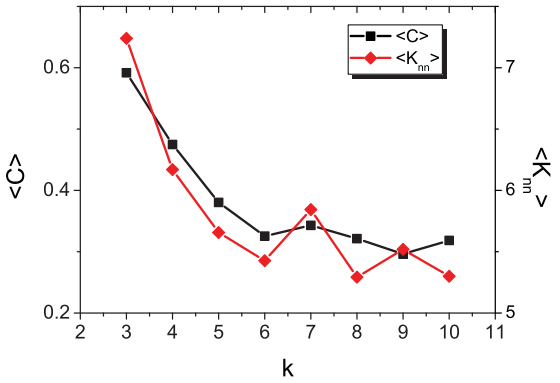


FIG. 3. (Color online) The distributions of $\langle C\rangle$ and $\langle k_{nn}\rangle$ as a function of $k$. Network is generated with $N = 3$.

investigate the community structure and modular architecture of the brain functional network with $N = 3$.

To better understand the architecture of the brain functional network $N = 3$, we study the average cluster coefficient $\langle C\rangle$ for vertices with degree $k$. Their relation reveals a negative correlation, which suggests that low-degree vertices generally belong to well-connected clusters while the neighbors of high-degree vertices belong to many different communities that are not directly connected among themselves, namely hierarchical organization (see Fig. 3). Meanwhile, the assortative mixing pattern (degree-degree correlation of vertices) is also investigated by using a measure of average nearest-neighbor degree $\langle K_{nn}\rangle$ that is defined as the average over vertices with degree $k$ (see Fig. 3). Degree mixing can be organized into two patterns: assortative behavior if $\langle K_{nn}\rangle$ increases with $k$, which indicates that high-degree vertices are preferentially connected with other high-degree vertices, and disassortative behavior if $\langle K_{nn}\rangle$ decreases with $k$, which denotes that links are more easily built between high-degree vertices and small ones [41]. In Fig. 3, we find that $\langle K_{nn}\rangle$ decreases with $k$, which indicates a disassortative behavior of brain functional network.

The community structure of brain functional network is further demonstrated by a dendrogram plot computed with the fast GN algorithms, as shown in Fig. 4. In Fig. 4(a), the number of communities corresponding to the maximum modularity is 20, which is marked by a dashed line. Thus, in Fig. 4(b), the dendrogram plot only shows hierarchical tree that splits the network into 20 communities. Note that we do not present the whole dendrogram plot so that the end points of hierarchical tree still denote communities that are randomly ordered with numeric labels from 1 to 20 in Fig. 4(b).

After analyzing the functional community structure of the EEG-channel network, we further investigate the relation between its functional community structure and its anatomical community structure (note that the anatomical community structure is performed in Tables I and II). We examine the overlap between community structures of brain functional networks and anatomical networks of the brain cortex in two ways. On the one hand, we check how many EEG channels of the same functional community belong to the same anatomical group, which is represented by the composition of communities written as

$$c(i,j) = |C(i) \cap G(j)|/|C(i)|. \tag{3}$$

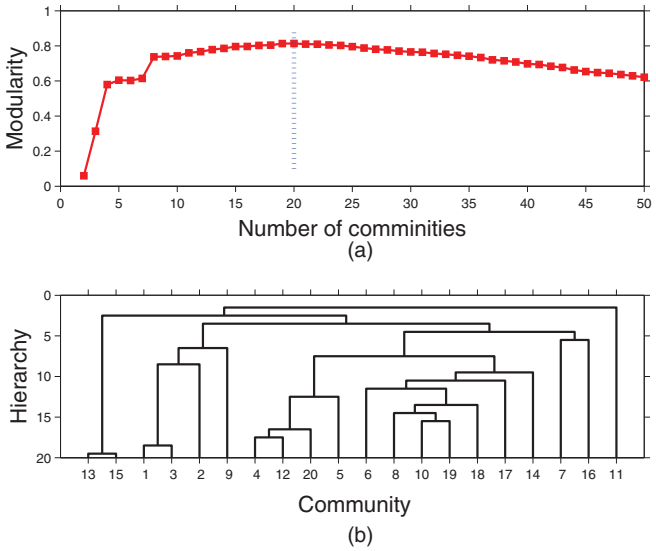


FIG. 4. (Color online) Modularity (a) and dendrogram plot (b) when network is generated with $N = 3$.

On the other hand, we investigate whether EEG channels of the same anatomical group are exactly clustered into an identical functional community, which is described by the participation of anatomical groups defined as

$$p(i,j) = |C(i) \cap G(j)|/|G(j)|. \tag{4}$$

In Eqs. (3) and (4), $C(i)$ and $G(j)$ denote the channel set of community $i$ and anatomical group $j$, respectively. If there is a perfect one-to-one correspondence between the two kinds community structures, we will have $c(i,i) = p(i,i) = 1$ and $c(i,j) = p(i,j) = 0$.

Figure 5(a) shows the composition of communities from different anatomical groups. This figure suggests that most functional communities are composed of EEG channels that are restricted to the same Brodmann area. For instance, community 12 (numeric label) almost overlaps with Brodmann area 9, i.e., the channels belonging to the same anatomical group are densely connected, or strongly coupled, in the corresponding brain functional network. In Fig. 5(b), the participation of anatomical group reveals that most of the channel sets restricted to the same Brodmann areas are clustered into the same functional community. In particular, Brodmann areas 10, 17, and 47 are completely overlapped with communities 20, 10, and 1 (numeric labels), respectively. It is noted that some channel sets of anatomical groups are divided into several large communities because Brodmann areas involved in these anatomical groups are distributed in both the left and right cerebral hemispheres with a much larger spatial distance. This reduces the coupling strength among the EEG channels. For instance, Brodmann area 21 is mainly divided into two larger communities with numeric labels 1 and 15, which are distributed in left and right cerebral hemispheres, respectively. This explains why the one-to-one correspondence between functional communities and anatomical groups is not perfect [i.e., $c(i,i), p(i,i) \neq 1$].

The bright diagonal in Fig. 5 indicates the significant correspondence between the community structure of functional networks from EEG time series and the anatomical

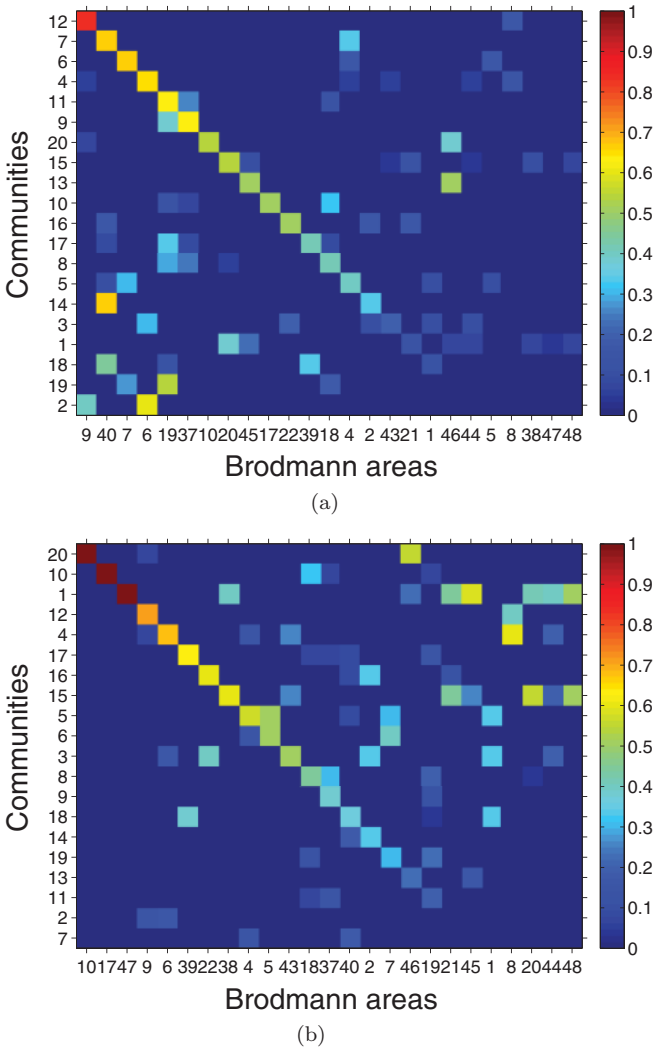


FIG. 5. (Color online) (a) Composition of communities from different anatomical groups. (b) Participation of anatomical groups in communities of functional networks (derived form EEG). The result reveals the coincidence between modular architectures of brain functional networks and anatomical groups based on anatomy parcellation of brain cortex. Network generated with $N = 3$ is divided into 20 communities. The communities and the Brodmann areas are arranged so the brightness of the diagonal drops from left to right.

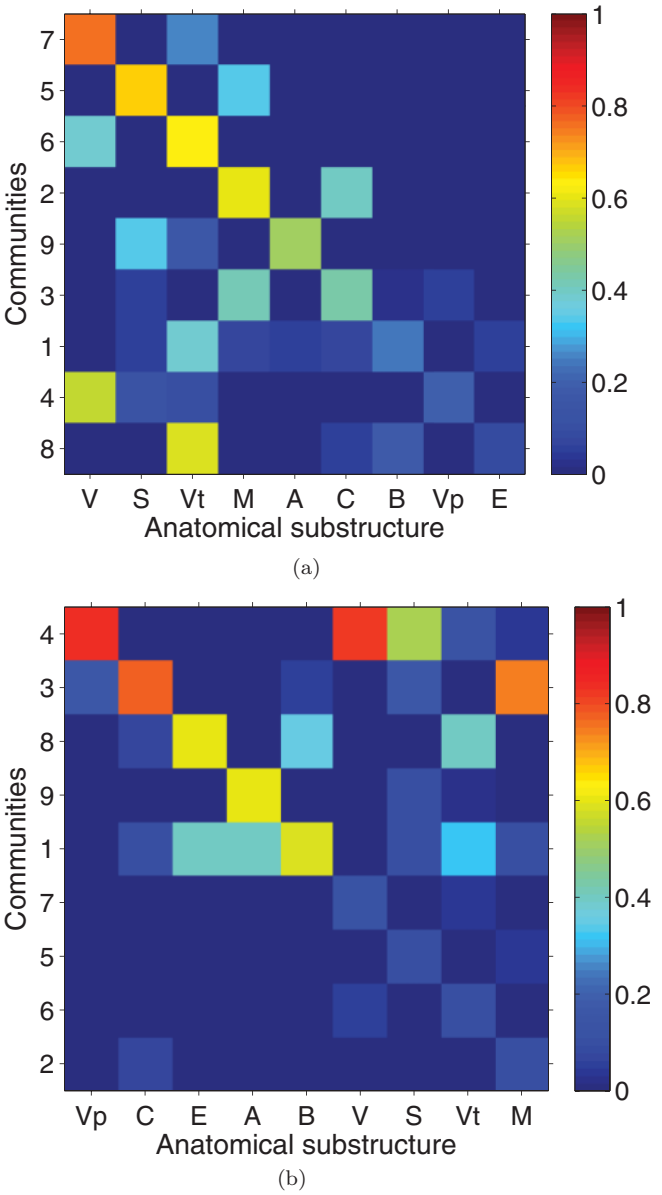


FIG. 6. (Color online) (a) Correspondence of community structure from functional networks (derived from EEG signal) to anatomical substructure networks (anatomical network) at a higher lever of hierarchy. (b) Participation of anatomical substructure in communities of brain functional networks (derived from EEG signal). The result shows the coincidence between modular architectures of brain functional network and anatomical substructure according to specific physiological functions of brain cortex. Network generated with $N = 3$ is divided into nine communities.

groups (by anatomical parcellations like the Brodmann areas) of the brain. Note that some regions in the diagonal in Fig. 5 are especially bright in color, suggesting an even more pronounced consistency between functional and anatomical structure in these areas. To see this more clearly, we examine this consistency at a larger scale, i.e., over a higher level of hierarchy. To do this we check the coincidence of modular architectures of brain functional network and anatomical substructures (i.e., a larger scale segmentation of the cortex which involves 9 larger anatomical communities, see Table II) in the same way. In Fig. 6(a) we can see that the diagonal is especially brighter at vision, sensory, vision-temporal, and motor cortices, indicating that the consistency between the modular structure of functional networks from the EEG signal and anatomical substructures is much higher at these four areas. This result is consistent with the visual task that involves visual, sensory, and motor functions of the brain. This result indicates that the synchronization among the EEG channels are much stronger in these anatomical substructures that are activated during the visual task. In Fig. 6(b), most of anatomical substructures are almost divided into unique communities, except for the visual-temporal part, which is symmetrically distributed in two hemispheres and is separated into two communities.

Figure 7(a) plots the averages of phase-coupling index between pairs of EEG channels within the same Brodmann

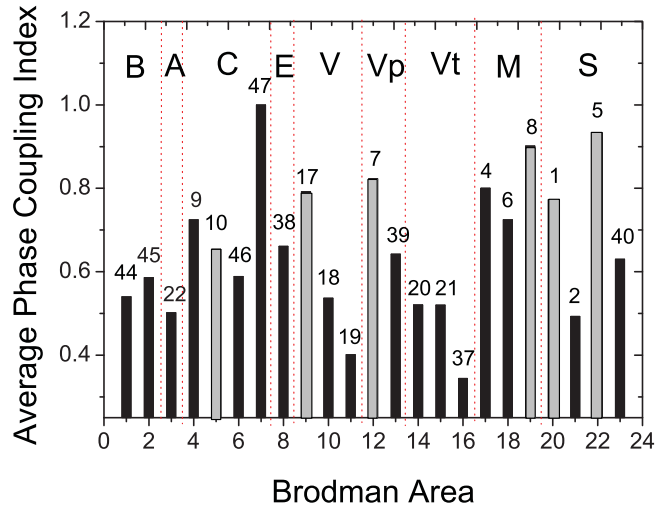


(a)

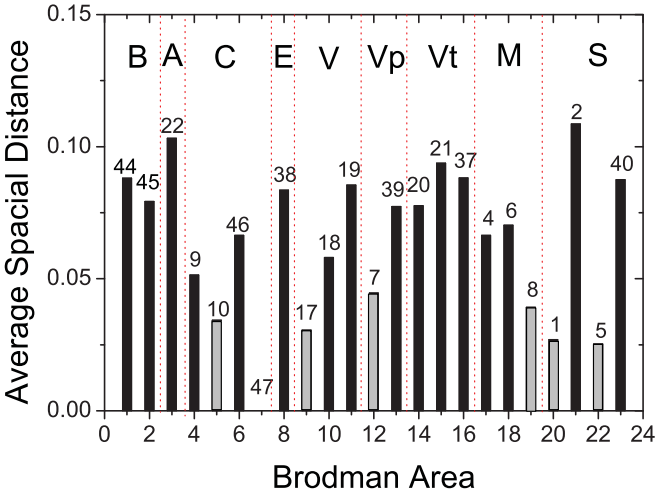


(b)

FIG. 7. (Color online) The averages of both phase-coupling index (a) and spatial distance (b) between pairs of EEG channels within the same Brodmann area. The Brodmann areas order according to the functional substructures in Table II, which are divided by the red dot line.

area. We find that the averages of phase-coupling index in all the Brodmann areas are mostly larger than 0.5. Specifically, the averages of phase-coupling index in the Brodmann areas 7, 17, 1, 5, 8 (correspond to the visual task that involves visual, sensory, and motor functions of brain) are significantly higher than other Brodmann areas belonging to the remaining anatomical substructures. The EEG channels tend to synchronize naturally among spatial neighbors due to the underlying sources affecting nearby channels fixed in the cerebral cortex. To further demonstrate that the observed high modularity in certain Brodmann areas is not an artifact of the spatial adjacency of the EEG electrodes, we also compute the averages of spatial distance $d$ between pairs of EEG channels in each Brodmann area, as shown in Fig. 7(b). We take Brodmann area 10 as a reference, because it has a similar $d$ with Brodmann areas 7, 17, 1, 5, and 8. Note that although Brodmann area 10 has a comparable $d$ with areas 7, 17, 1, 5, and 8, the averages phase-coupling index of the former is significantly lower than those from the latter (note specifically that Brodmann area 10 has a smaller $d$ than Brodmann area 7, while its average phase index is much smaller that that of Brodmann area 7), which suggests that the high phase-coupling index, and thus high modularity, of Brodmann areas 7, 17, 1, 5, and 8 is not due to the spatial adjacency of the EEG electrodes in these Brodmann areas. The pronounced consistency between the modular structures of the functional and the anatomical network in these Brodmann areas, therefore, is essentially due to the performed task.

In addition, the electrical activity of neuronal networks is known to oscillate at various frequencies and amplitudes. The strongly correlated oscillators in same communities will synchronize more easily than those in different communities, which suggests that the synchronization reveals hierarchical organization for a network with a nontrivial community structure [42–47]. Moreover, the simulation of neuronal activity based on anatomical cat brain network determines that the correlated clusters are consistent with anatomical areas of same brain functions [48–50]. Thus, the coincidence of modular architectures of brain functional networks and the anatomical groups of brain cortex at two levels of hierarchy suggests that the correlation of the EEG time series in same anatomical groups is much stronger than that of the EEG time series in different anatomical groups and the hierarchical organization of the brain functional network may be a consequence of the functional segmentation of the brain cortex.

## IV. CONCLUSION

In conclusion, we have investigated the hierarchical modular organizations of the brain functional network that are derived from the extent of phase synchronization among high-resolution synchronous EEG time series during the visual task. The resulting brain functional networks show common small-world property and community structure organized in a hierarchical way. Meanwhile, by clustering EEG channels into functional communities and comparing it to the anatomical parcellation of brain cortex, we find that the modular architecture of brain functional networks corresponds well to that of the anatomical groups over different levels of hierarchy, and this consistency is more pronounced at vision, sensory, vision-temporal, motor cortices, which involve vision, sensory, and motor functions of the brain during the visual task. These interesting results suggest that the strong modularity in vision and other related cortices forms the functional basis in these areas and the structure-function relationship further reveals that the strong synchronization among EEG channels within the functional communities may be a consequence of functional segmentation of brain cortex.

## ACKNOWLEDGMENTS

This work is supported by the National Natural Science Foundation of China under Grant Nos. 60874090, 60974079, and 61004102. S.-M.C. appreciates the financial support of the K.C. Wong Education Foundation, China Postdoctoral Science Foundation (No. 20100480704), and

the Fundamental Research Funds for the Central Universities (No. WK2100230004). J.-Z. acknowledges the support from Natural Scientific Foundation of China under Grant Nos. 61004104 and 61104143.

[1] S. R. Cajal, *Histology of the Nervous System of Man and Vertebrates* (Oxford University Press, New York, 1995).
[2] L. W. Swanson, *Brain Architecture* (Oxford University Press, Oxford, 2003).
[3] G. Deco, V. K. Jirsa, and A. R. Mclntosh, Nat. Rev. Neurosci. **12**, 43 (2011).
[4] E. Bullmore and O. Sporns, Nat. Rev. Neurosci. **10**, 186 (2009).
[5] D. J. Watts and S. H. Strogatz, Nature **393**, 440 (1998).
[6] A. L. Barabási and R. Albert, Science **286**, 509 (1999).
[7] C. J. Stam, Neurosci. Lett. **355**, 25 (2004).
[8] V. M. Eguiluz, D. R. Chialvo, G. A. Cecchi, M. Baliki, and A. V. Apkarian, Phys. Rev. Lett. **94**, 018102 (2005).
[9] D. S. Bassett and E. Bullmore, The Neuroscientist **12**, 512 (2006).
[10] S. Achard, R. Salvador, B. Whitcher, J. Suckling, and E. Bullmore, J. Neurosci. **26**, 63 (2006).
[11] M. P. Van den Heuvel, C. J. Stam, M. Boersma, and H. E. Hulshoff Pol, NeuroImage **43**, 528 (2008).
[12] G. L. Gong, Y. He, L. Concha, C. Lebel, D. W. Gross, A. C. Evans, and C. Beaulieu, Cereb. Cortex **19**, 524 (2009).
[13] M. E. J. Newman and M. Girvan, Phys. Rev. E **69**, 026113 (2004).
[14] D. M. Wilkinson and B. A. Huberman, Proc. Natl. Acad. Sci. USA **101**, 5241 (2004).
[15] P. F. Jonsson, T. Gavanna, D. Zicha, and P. A. Bates, BMC Bioinf. **7**, 2 (2006).
[16] S. M. Cai, Y. B. Zhou, T. Zhou, and P. L. Zhou, Int. J. Mod. Phys. B **21**, 433 (2010).
[17] M. Girvan and M. E. J. Newman, Proc. Natl. Acad. Sci. USA **99**, 7821 (2002).
[18] A. Capocci, V. D. P. Servedio, G. Caldarelli, and F. Colaiori, Physica A **352**, 669 (2005).
[19] A. Arenas, A. Fernández, and S. Gómez, New J. Phys. **10**, 053039 (2008).
[20] J. Zhang, K. Zhang, X. Xu, C. K. Tse, and M. Small, New J. Phys. **11**, 113003 (2009).
[21] J. Zhang, C. Zhou, X. Xu, and M. Small, Phys. Rev. E **82**, 026116 (2010).
[22] K. Zhang, I. W. Tsang, and J. T. K. Kwok, IEEE Trans. Neural Networks **20**, 583 (2009).
[23] K. Zhang and J. T. K. Kwok, IEEE Trans. Neural Networks **21**, 644 (2010).
[24] S. Fortunato, Phys. Rep. **486**, 75 (2010).
[25] R. Salvador, J. Suckling, M. R. Coleman, J. D. Pickard, D. Menon, and E. Bullmore, Cereb. Cortex **15**, 1332 (2005).
[26] L. Ferrarini *et al.*, Hum. Brain Map. **30**, 2220 (2009).
[27] M. Chavez, M. Valencia, V. Navarro, V. Latora, and J. Martinerie, Phys. Rev. Lett. **104**, 118701 (2010).
[28] Introduction to Brodmann area [http://en.wikipedia.org/wiki/Brodmann_area].
[29] A Human Electrophysiology Data Resource [http://sccn.ucsd.edu/eeglab/data/headit.html].
[30] S. Makeig, M. Westerfield, T. P. Jung, S. Enghoff, J. Townsend, E. Courchesne, and T. J. Sejnowski, Science **295**, 690 (2002).
[31] S. Makeig, A. Delorme, M. Westerfield, T. P. Jung, J. Townsend, E. Courchense, and T. J. Sejnowski, PLOS Biology **2**, 742 (2004).
[32] Y. Kuramoto, *Chemical Oscillations, Waves, and Turbulence* (Springer, Berlin, 1984).
[33] M. K. Stephen Yeung and S. H. Strogatz, Phys. Rev. Lett. **82**, 648 (1999).
[34] M. Timme, F. Wolf, and T. Geisel, Phys. Rev. Lett. **89**, 258701 (2002).
[35] D. Gabor, J. IEE London **93**, 429 (1946).
[36] B. Schelter, M. Winterhalder, R. Dahlhaus, J. Kurths, and J. Timmer, Phys. Rev. Lett. **96**, 208103 (2006).
[37] J. Nawrath, M. C. Romano, M. Thiel, I. Z. Kiss, M. W. Wickramasinghe, J. Timmer, J. Kurths, and B. Schelter, Phys. Rev. Lett. **104**, 038701 (2010).
[38] X. Xu, J. Zhang, and M. Small, Proc. Natl. Acad. Sci. **105**, 19601 (2008).
[39] Introduction to MRIcro [http://www.sph.sc.edu/comd/rorden/mricro.html].
[40] Download software from website [http://www.fil.ion.ucl.ac.uk/spm/software/spm8/].
[41] X.-K. Xu, J. Zhang, and M. Small, Phys. Rev. E **82**, 046117 (2010).
[42] A. Arenas, A. Diaz-Guilera, and C. J. Perez-Vicente, Phys. Rev. Lett. **96**, 114102 (2006).
[43] C. S. Zhou and J. Kurths, Chaos **16**, 015104 (2006).
[44] J. Gomez-Gardenes, Y. Moreno, and A. Arenas, Phys. Rev. Lett. **98**, 034101 (2007).
[45] A. Arenas and A. Dıaz-Guilera, Eur. Phys. J. B **143**, 19 (2007).
[46] G. Yan, Z.-Q. Fu, J. Ren, and W. X. Wang, Phys. Rev. E **75**, 016108 (2007).
[47] A. Arenas, A. Díaz-Guilera, J. Kurths, Y. Moreno, and C. S. Zhou, Phys. Rep. **469**, 93 (2008).
[48] C. Zhou, L. Zemanová, G. Zamora, C. C. Hilgetag, and J. Kurths, Phys. Rev. Lett. **97**, 238103 (2006).
[49] L. Zemanová, C. S. Zhou, and J. Kurths, Physica D **224**, 202 (2006).
[50] C. S. Zhou, L. Zemanová, G. Z. López, C. C. Hilgetag, and J. Kurths, New J. Phys. **9**, 178 (2007).